Whereas it is quite plausible that (A) represents a time history which will be generated when diagram (b) of (5.97) is iterated in the Lippmann-Schwinger equation, one might naively be tempted to regard (B) as a valid four-particle three-hole contribution to the optical potential. Clearly, the derivation shows it must not be included, which is associated with the fact that the Lippman Schwinger equation has no projector onto states above the Fermi surface and thus generates propagation in hole states as well as particle states.

5.4 LINEAR RESPONSE

THE RESPONSE FUNCTION

Section 2.1 showed how experimental observables could be expressed in terms of response functions, which we will now write in terms of two-particle Green's functions. To obtain the product of two one-body operators, we must consider a two-particle Green's function in which the creation operators are evaluated infinitesimally later than the annihilation operators and we define the density-density correlation function and its retarded counterpart as

$$\begin{aligned}\overline{D}(1,2) &\equiv iG^{(2)}(1\,2|1^+\,2^+) = -i\langle T\hat{\phi}^\dagger(1)\hat{\phi}(1)\hat{\phi}^\dagger(2)\hat{\phi}(2)\rangle \\ \overline{D}_R(1,2) &\equiv -i\theta(t_1-t_2)\langle[\hat{\phi}^\dagger(1)\hat{\phi}(1),\,\hat{\phi}^\dagger(2)\hat{\psi}(2)]\rangle\ .\end{aligned} \tag{5.99}$$

As in Section 5.2, a spectral representation is obtained by inserting a complete set of states and Fourier transforming. For brevity, we will only write the zero temperature results, and leave the analogous finite temperature expressions as a straightforward exercise:

$$\begin{aligned}\left\{\begin{matrix}\overline{D}(x_1,x_2;\omega)\\ \overline{D}_R(x_1,x_2;\omega)\end{matrix}\right\} = \sum_n \Bigg[&\frac{\langle\psi_0|\hat{\rho}(x_1)|\psi_n^N\rangle\langle\psi_n^N|\hat{\rho}(x_2)|\psi_0\rangle}{\omega-(E_n^N-E_0)+i\eta} \\ &- \frac{\langle\psi_0|\hat{\rho}(x_2)|\psi_n^N\rangle\langle\psi_n^N|\hat{\rho}(x_1)|\psi_0\rangle}{\omega+(E_n^N-E_0)\mp i\eta}\end{aligned} \tag{5.100}$$

where the density operator is written $\psi^\dagger(x_1)\psi(x_1) \equiv \hat{\rho}(x_1)$. In momentum space, using

$$\begin{aligned}\hat{\rho}(q) &= \int e^{-iq\cdot x}\rho(x) \\ &= \int e^{-iq\cdot x}\left[\int \frac{d^3k}{(2\pi)^3}e^{-ik\cdot x}a_k^\dagger\right]\left[\int\frac{d^3k'}{(2\pi)^3}e^{+ik'\cdot x}a_{k'}\right] \\ &= \int\frac{d^3k}{(2\pi)^3}a_k^\dagger a_{k+q}\ . \\ \hat{\rho}(q)^\dagger &= \hat{\rho}(-q)\end{aligned} \tag{5.101}$$

we obtain

$$\left\{\begin{matrix}\overline{D}(k,\omega)\\ \overline{D}_R(k,\omega)\end{matrix}\right\} = \sum_n\left[\frac{|\langle\psi_n^N|\hat{\rho}(-q)|\psi_0\rangle|^2}{\omega-(E_n^N-E_0)+i\eta} - \frac{|\langle\psi_n^N|\hat{\rho}(q)|\psi_0\rangle|^2}{\omega+(E_n^N-E_0)\mp i\eta}\right]\ . \tag{5.102}$$

The essential difference relative to Eq. (5.27) is the presence of N-particle intermediate states rather than states with $N\pm1$ particles, so that the density-density response function contains information about the eigenstates of the N-particle system itself.

From Eq. (5.100), it is evident how to calculate the observables discussed in Section 2.1. First $\overline{D}$ is calculated in an appropriate approximation using the perturbation theory we have derived for the Green's function G_2. A response function, Eq. (2.16), is then evaluated by calculating $\overline{D}_R$ from the relations

$$\begin{aligned}\mathrm{Re}\,\overline{D}(\omega) &= \mathrm{Re}\,\overline{D}_R(\omega) \\ \mathrm{Im}\,\overline{D}(\omega) &= \mathrm{sgn}(\omega-E_0)\,\mathrm{Im}\,\overline{D}_R\ .\end{aligned} \tag{5.103}$$

Analogous expressions can, of course, be written with an arbitrary one-body operator replacing the density operator. Similarly, the inclusive scattering cross section, Eq. (2.19) can be evaluated from the imaginary part of $\overline{D}$, since only the first term in Eq. (5.100) or (5.102) contributes for positive ω:

$$\begin{aligned}\sigma(q,\omega) &= 2\pi\sum_n\delta(E_n^N-E_0-\omega)\tilde{v}(q)^2|\langle\psi_n^N|\hat{\rho}(-q)|\psi_0\rangle|^2 \\ &= -2\mathrm{Im}\,\overline{D}(q,\omega)\tilde{v}(q)^2\ .\end{aligned} \tag{5.104a}$$

Because of its direct relation to experiment, the imaginary part of the response function is often referred to as the dynamic structure factor:

$$S(q,\omega) \equiv -\mathrm{Im}\,\overline{D}(q,\omega) = \frac{\sigma(q,\omega)}{2\tilde{v}(q)^2}\ . \tag{5.104b}$$

Finally, it is convenient and conventional to define the density fluctuation operator

$$\tilde{\rho} - \hat{\rho} - \langle\hat{\rho}\rangle \tag{5.105}$$

and its correlation functions

$$\begin{aligned}iD(1,2) &= \langle T\tilde{\rho}(1)\tilde{\rho}(2)\rangle \\ &= \langle T\hat{\psi}^\dagger(1)\hat{\psi}(1)\ \hat{\psi}^\dagger(2)\hat{\phi}(2)\rangle - \langle T\hat{\psi}^\dagger(1)\hat{\psi}(1)\rangle\langle T\hat{\psi}^\dagger(2)\psi(2)\rangle \\ &= i\overline{D}(1,2) - \langle\hat{\rho}(1)\rangle\langle\hat{\rho}(2)\rangle \\ iD_R(1,2) &= \theta(t_1-t_2)\langle[\tilde{\rho}(1),\ \tilde{\rho}(2)]\rangle = i\overline{D}_R(1,2)\ .\end{aligned} \tag{5.106a, 5.106b}$$

Note that $D_R = \overline{D}_R$ since $\langle\hat{\rho}\rangle$ does not contribute to the commutator and that $\sigma(q,\omega) = -2\mathrm{Im}\,D(k,\omega)\tilde{v}^2(q)$ because $\langle\hat{\rho}\rangle$ does not connect $|\psi_0\rangle$ to any excited states in (5.104). The fluctuation-dissipation theorem is particularly clear in this language, since transport coefficients are specified by the expectation value of products of fluctuation operators. The advantage of Eq. (5.106a) is the fact that its diagram expansion contains all liked diagrams which connect the density operators at points 1 and 2. Taken by itself, $\overline{D}(1,2)$ contains linked diagrams of two generic types, those which connect the operators at 1 and 2 and those which do not:

$\overline{D}(1,2) =$ 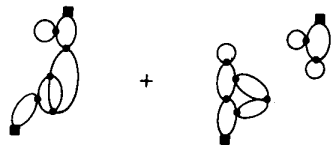 (5.107)

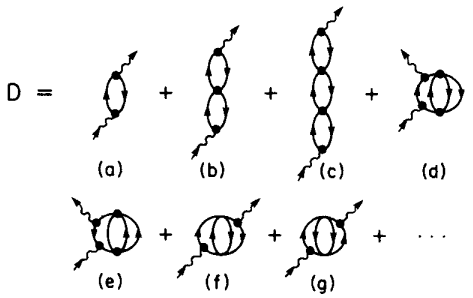

Fig. 5.10 Feynman diagrams for the response function D. Action of the density operators $\tilde{\rho}(1)$ and $\tilde{\rho}(2)$ are denoted by and which in momentum space may be regarded as injecting momentum $\vec{q}$ at (1) and removing it at (2). Note that in addition to the diagrams shown, the contributions through second order also include Hartree-Fock self-energy insertions on the propagators in diagrams (a) and (b).

The disconnected pieces in Eq. (5.107) simply correspond to all diagrams in the product $\langle\hat{\rho}(1)\rangle\langle\hat{\rho}(2)\rangle$ which are precisely subtracted off in $D(1, 2)$. Feynman diagrams corresponding to the first few orders of perturbation theory for $D(1, 2)$ are shown in Fig. 5.10.

The diagram rules for D follow immediately from the definition Eq. (5.99) and the zero-temperature Feynman rules of Section 4.1. Recall that i^2G_2 has propagators iG_0 for each line and the overall factor $(-i)^r(-1)^P(-1)^{n_L}$ where r is the number of interactions, n_L is the number of internal closed loops and $(-1)^P$ is the sign of the permutation of the external legs. For the identity permutation in which 1 connects to $1'$ and 2 connects to $2'$ the diagram for D has two additional closed loops relative to G_2. For all other permutations, connecting 1 to $2'$ and 2 to $1'$ creates one additional closed loop in D relative to G_2. Thus, associating a minus sign with every closed loop in D correctly accounts for both the factors $(-1)^P$ and $(-1)^{n_L}$. To include direct and exchange interactions on an equal footing as in Fig. 5.10, we will use Hugenholtz diagrams and include the factor $\frac{1}{2^{n_e}}$ for equivalent lines. Including the explicit i in the definition (5.99), the overall factor for a diagram contributing to D is $(-i)^{r+1}(-1)^{n'_L}\frac{1}{2^{n_e}}$ where r is the number of interactions, n'_L is the total number of closed loops in a diagram when it is drawn with direct matrix elements, and n_e is the number of equivalent lines. The propagators in the diagram are iG_0 and the interactions are antisymmetrized matrix elements $\{k_1\,k_2|v|k_3\,k_4\}$.

Additional insight into the physical content of the response function is obtained by considering the set of time-ordered diagrams corresponding to each Feynman diagram. For convenience, we will treat a translationally-invariant system and enumerate a complete set of multi-particle, multi-hole states. Let us write the amplitude for producing each intermediate state by injecting momentum q into the ground state as a sum of time-ordered diagrams, so that the matrix element $|\langle\psi_n^N|\hat{\rho}|\psi_0\rangle|^2$ is given by all possible pairs of one diagram from the set connected with the adjoint of another diagram from the same set. For example, the top line of Fig. 5.11 shows four time-histories leading

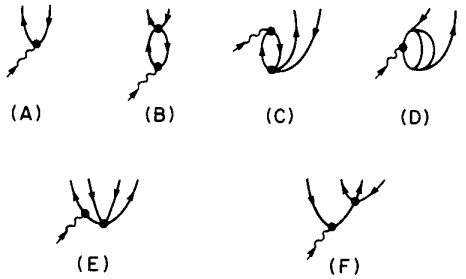

Fig. 5.11 Time-ordered diagrams for amplitudes contributing to the response function.

to a one-particle one-hole state. If diagram (A) is connected to $(A^\dagger)$, which is the same diagram drawn upside down, we obtain one time order of diagram (a) of Fig. 5.10 in which a one-particle one-hole excitation is first created and then destroyed by the action of $\vec{q}$. In the language of scattering theory, diagrams (B) and (C) would be called final-state and initial state interaction corrections, respectively. Note how the cross terms between {A, B, C} and { $A^\dagger$ $B^\dagger$ $C^\dagger$} produce various time orders of the "chain" diagrams (a), (b), and (c), so that initial and final state interaction effects become totally entangled in the response function. Similarly, for the two-particle two-hole states in the second line, combining (E) with $(F^\dagger)$ yields particular time-orders (d) and (g), but diagram (g) is also obtained by combining (D) and $(A^\dagger)$. Thus, it is clear that the Feynman diagram expansion of the response function provides an economical description of a complicated process. The interplay of initial and final state interactions is treated consistently and the combinatoric of obtaining the same contribution from products of distinct amplitudes is automatically summarized by the rule that all symmetry factors are one for any Green's function. The flexibility to treat the response function in terms of time-ordered diagrams as well as Feynman diagrams may be exploited in specific applications, such as studying the scaling behavior of the response function at high momentum transfer (see Problem 4).

RANDOM PHASE APPROXIMATION

Any practical calculation of the response function must truncate the infinite diagram expansion. One alternative to simply stopping at some specific order of perturbation theory is to sum an appropriate infinite series of diagrams. Summing the set of all chain diagrams, the first three elements of which are shown in (a) – (c) of Fig. 5.10 yield the so-called random phase approximation or RPA. (Actually, there are two distinct approximations which are commonly referred to as the RPA: the present treatment of the response function and the summation of the ring diagram contributions, Eqs. (2.113) – (2.115) to the ground state correlation energy. The RPA correlation energy is treated in Problems 5.5 and 5.7.)

As a prelude to summing chains, let us first calculate a single link, diagram (a) of Fig. 10, which corresponds to the response function D_0 for a non-interacting system. For simplicity, we will treat a translationally invariant system in momentum space and assume spin-1/2 Fermions. Noting that diagram (a) has a closed loop, no interactions,

no equivalent lines and two propagators iG_0, we obtain the contribution

$$D_0(q,\omega) = \quad \overset{k+q}{\bigcirc}\!\!\!\!\!\!\bigcirc \overset{k}{} \quad \begin{matrix} q \\ q \end{matrix}$$

$$= -2i\int \frac{d^3k d\omega_k}{(2\pi)^4} G_0(k+q,\omega_k+\omega)G_0(k,\omega_k) \tag{5.108}$$

$$= -2i\int \frac{d^3k d\omega_k}{(2\pi)^4}\left(\frac{1-n_{k+q}}{\omega_k+\omega-\epsilon_{k+q}+i\eta}+\frac{n_{k+q}}{\omega_k+\omega-\epsilon_{k+q}-i\eta}\right)$$

$$\times\left(\frac{1-n_k}{\omega_k-\epsilon_k+i\eta}+\frac{n_k}{\omega_k-\epsilon_k-i\eta}\right)$$

$$= 2\int \frac{d^3k}{(2\pi)^3}\left[\frac{(1-n_{k+q})n_k}{\omega+\epsilon_k-\epsilon_{k+q}+i\eta}-\frac{n_{k+q}(1-n_k)}{\omega+\epsilon_k-\epsilon_{k+q}-i\eta}\right] .$$

Performing the momentum integrals in Eq. (5.108) with the zero-temperature occupation numbers $n_k = \theta(k_F - |k|)$ as outlined in Problem 5.6 yields the Lindhard function (Lindhard, 1954)

$$\mathrm{Re}\, D_0(\vec{q},\omega) = \frac{mk_F}{2\pi^2}\left\{-1+\frac{1}{2\tilde{q}}\left[1-\left(\frac{\tilde{\omega}}{\tilde{q}}-\frac{\tilde{q}}{2}\right)^2\right]\ln\left|\frac{1+\left(\frac{\tilde{\omega}}{\tilde{q}}-\frac{\tilde{q}}{2}\right)}{1-\left(\frac{\tilde{\omega}}{\tilde{q}}-\frac{\tilde{q}}{2}\right)}\right|\right.$$

$$\left.-\frac{1}{2\tilde{q}}\left[1-\left(\frac{\tilde{\omega}}{\tilde{q}}+\frac{\tilde{q}}{2}\right)^2\right]\ln\left|\frac{1+\left(\frac{\tilde{\omega}}{\tilde{q}}+\frac{\tilde{q}}{2}\right)}{1-\left(\frac{\tilde{\omega}}{\tilde{q}}+\frac{\tilde{q}}{2}\right)}\right|\right\} \tag{5.109a}$$

$$\mathrm{Im}\, D_0(\vec{q},\omega) = \left\{\begin{matrix} -\frac{mk_F}{4\pi\tilde{q}}\left[1-\left(\frac{\tilde{\omega}}{\tilde{q}}-\frac{\tilde{q}}{2}\right)^2\right] & \left|\frac{\tilde{q}}{2}-\tilde{q}\right| \le \tilde{\omega} \le \frac{\tilde{q}}{2}+\tilde{q} \\ -\frac{mk_F}{4\pi\tilde{q}}2\tilde{\omega} & 0 \le \tilde{\omega} \le \tilde{q}-\frac{\tilde{q}^2}{2} \end{matrix}\right\} \tag{5.109b}$$

where

$$\tilde{q} \equiv \frac{q}{k_F} , \qquad \tilde{\omega} \equiv \frac{\omega m}{k_F^2} . \tag{5.109c}$$

The imaginary part, which specifies the inclusive cross section, Eq. (5.104), for a non-interacting Fermi gas has a very simple physical interpretation: it simply counts the ways an occupied state $|\vec{k}| < k_F$ can be scattered to an unoccupied state $|\vec{k}+\vec{q}| > k_F$ by transferring momentum $\vec{q}$ and energy $\omega = \epsilon_{k+q} - \epsilon_k = \frac{\vec{k}\cdot\vec{q}}{m} + \frac{q^2}{2m}$. For $q > 2k_F$, the Fermi sphere conditions are satisfied for all $k < k_F$, so as sketched in Fig. 5.12a, the extremal values $\omega = \frac{q^2}{2m} \pm \frac{qk_F}{m}$ are obtained for $|\vec{k}| = k_F$ and $\vec{k}$ aligned with or opposite to $\vec{q}$. The maximum occurs for $\vec{k}$ perpendicular to $\vec{q}$ corresponding to $\omega = \frac{q^2}{2m}$ since all transverse values of $|\vec{k}| < k_F$ can contribute in this case. For $q < 2k_F$, the result is sketched in Fig. 5.12b. Whereas at large ω, one has the same parabola as in

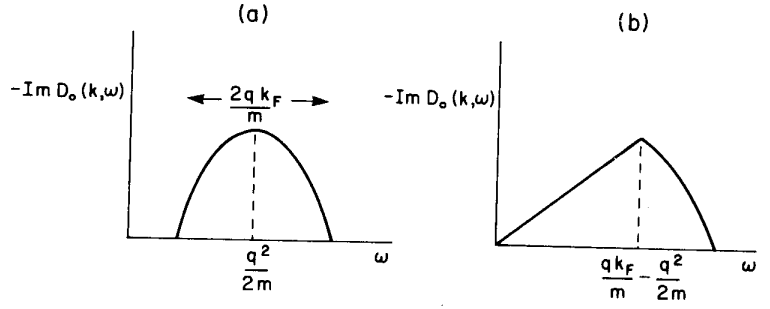

Fig. 5.12 Imaginary part of the response function $D_0(k,\omega)$ for $q > 2k_F$ (a) and $q < 2k_F$ (b).

case (a), at $\omega = \frac{qk_F}{m} - \frac{q^2}{2m}$ the simultaneous requirements $|\vec{k}| < k_F$ and $|\vec{k}+\vec{q}| > k_F$ further restrict the phase space, yielding the linear behavior shown for lower ω.

We may now sum the sequence of chain diagrams contributing to the response function by writing an integral equation which iterates the addition of a single link. Let $G^{\mathrm{ph}}(k_1+q,\ k_1|k_2+q,\ k_2;\omega)$ denote the particle-hole Green's function obtained by separating the pairs of creation and annihilation operators which correspond to the external density operator in $D(q,\omega)$:

$$G^{\mathrm{ph}}(k_1+q,k_1|k_2+q,k_2;\omega) \equiv \quad \begin{matrix} k_2+q & k_1 \\ \square & \\ k_2+q & k_2 \end{matrix}$$

$$\equiv -i\int d(t_1-t_2)e^{i\omega(t_1-t_2)}\left\{\langle T a^\dagger_{k_1}(t_1)a_{k_1+q}(t_1)a^\dagger_{k_2+q}a_{k_2}(t_2)\rangle\right. \tag{5.110}$$

$$\left.-\langle a^\dagger_{k_1}a_{k_1+q}\rangle\langle a^\dagger_{k_2+q}a_{k_2}\rangle\right\}$$

with the property

$$D(q,\omega) = \sum_{k_1k_2} G^{\mathrm{ph}}(k_1+q,k_1|k_2+q,k_2;\omega) . \tag{5.111}$$

Here and throughout this section where no ambiguity will arise, we abbreviate momentum integrals and spin sums by $\sum_k = \int \frac{d^3k}{(2\pi)^3}\sum_\sigma$ and neglect the normalization volume $\mathcal{V}$ which cancels out of all observables.

Chain diagrams are summed by the following integral equation which yields the particle-hole Green's functions in the random-phase approximation

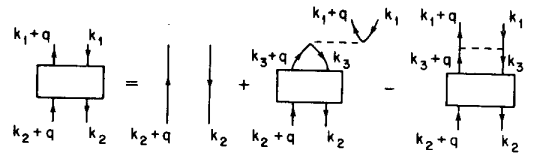

(5.112a)

The first term on the right-hand side is the particle-hole Green's function for the non-interacting system, and by definition, it is identical to D_0 in Eq. (5.108) except for the absence of the momentum sum $\sum_k$. The direct and exchange terms are written explicitly so that one may observe that the direct term has the following factors in addition to the potential and $G^{\rm ph}_\Lambda$: $(-i)$ for the interaction, (-1) for the addition of a closed loop and iG_0 for each of two propagators. Since these factors are just those in D_0, the equation may be written

$$G^{\rm RPA}(k_1+q,\ k_1|k_2+q,k_2;\omega) = \left[\frac{(1-n_{k_1+q})n_{k_1}}{\omega+\epsilon_{k_1}-\epsilon_{k_1+q}+i\eta} - \frac{(1-n_{k_1})n_{k_1+q}}{\omega+\epsilon_{k_1}-\epsilon_{k_1+q}-i\eta}\right] \times \left[\delta_{k_1k_2} + \sum_{k_3}\{k_3,k_1+q|v|k_3+q,k_1\}\, G^{\rm RPA}(k_3+q,k_3|k_2+q,k_2;\omega)\right] \quad . \tag{5.112b}$$

This equation clearly has the general structure of the integral equation discussed in Section 2.4 and in fact corresponds to the Bethe Salpeter equation in the particle-hole channel with the vertex function approximated by the bare interaction. We will return to the more general case in Chapter 6 in connection with Landau Fermi liquid theory.

The direct matrix element in Eq. (5.112b) only depends on the momentum transfer q, $\langle k_3, k_1+q|v|k_3+q,k_1\rangle = \tilde{v}(-q)$ whereas the exchange matrix element $\tilde{v}(k_3-k_1)$ depends on the internal momenta. Hence, when it is physically justified to neglect the exchange term, the RPA equation becomes a simple algebraic equation. There are several circumstances under which the exchange term may be neglected. First, consider the Coulomb potential, for which the direct and exchange terms are $\frac{e\pi e^2}{q^2}$ and $\frac{4\pi e^2}{|k_1-k_3|^2}$, respectively. For small q, the conditions that $|k_i+q| > k_F$ and $|k_i| < k_F$ or vice versa force $|k_1| \sim k_F$ so the direct term generally dominates the exchange term by the factor $\left(\frac{k_F}{q}\right)^2$. A second example is use of the high-spin technique to treat Bosons, in which case the direct term dominates the exchange term by the factor N. A specific application to the correlation energy of the dilute Bose gas is given in Problem 5.7. Finally, in any system such that the momentum dependence of the potential is negligible between 0 and $2k_F$, the exchange term may be effectively included with the direct term. An example is the response function for the one-dimensional δ-function interaction in Problem 5.8.

The sum of all direct RPA chain diagrams is obtained by multiplying Eq. (5.112b) by $\tilde{v}(q)$, summing over k, and dropping all exchange terms, with the result

$$G^{\rm RPA}(k_1+q,k_1|k_2+q,k_2;\omega) = G^{\rm ph}_0(k_1;q,\omega)\left[\delta_{k_1k_2} + \frac{\tilde{v}(q)G^{\rm ph}_0(k_2;q,\omega)}{1-\tilde{v}(q)D_0(q,\omega)}\right] \tag{5.113}$$

where we have denoted the particle-hole Green's functions for the non-interacting system, which is the first term in Eq. (5.112b), by

$$G^{\rm ph}_0(k;q,\omega) \equiv \frac{(1-n_{k+q})n_k}{\omega+\epsilon_k-\epsilon_{k+q}+i\eta} - \frac{(1-n_k)n_{k+q}}{\omega+\epsilon_k-\epsilon_{k+q}-i\eta} \tag{5.114a}$$

and

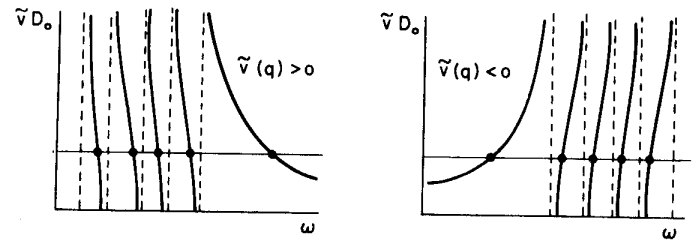

Fig. 5.13 Graphical solution for the RPA modes. The vertical asymptotes correspond to the particle-hole excitations $\omega = \epsilon_{k+q} - \epsilon_q$ and the curves show the qualitative behavior of $\tilde{v}(q)D_0(q,\omega)$ for the repulsive and attractive potentials, respectively.

$$D_0(q,\omega) = \sum_k G^{\rm ph}_0(k;q,\omega) \quad . \tag{5.114b}$$

Since the poles of $G^{\rm ph}$ (or D which is obtained by summing over k_1 and k_2) give the excited states of the system, in the random-phase approximation the excited states occur at ω such that

$$\tilde{v}(q)D_0(q,\omega) = 1 \quad . \tag{5.115}$$

To understand the structure of Eq. (5.115), it is useful to consider the graphical solutions sketched in Fig. 5.13. Since $D_0(q,\omega)$ is symmetric in ω (see Problem 5.6), it suffices to consider positive ω. For every value of $\vec{k}$ inside the Fermi sea such that $\vec{k}+\vec{q}$ is outside the Fermi sea, the first term in Eq. (5.114a) has a pole at $\omega = \epsilon_{k+q} - \epsilon_k$. For each $\vec{k}$ in the sum contributing to $D_0(q,\omega)$, asymptotes are plotted in Fig. 5.13, and $D_0(q,\omega)$ is a decreasing function between each pair of asymptotes. Thus, for a repulsive potential the solution to (5.115) is as sketched in the left part of Fig. 5.13. All except one of the solutions are trapped between states in the particle-hole continuum, and the remaining collective state is pushed above the highest state. Similarly, for an attractive potential, the collective state is brought down below the lowest particle-hole state.

In order to study the collective RPA modes in several physical systems at low q, it is useful to note the following behavior of $D_0(q,\omega)$ from Eq. (5.109)

$$\mathrm{Re}\, D_0(q,\omega) \underset{q\to 0}{\longrightarrow} \begin{cases} \frac{k_F^3}{3\pi^2 m}\frac{q^2}{\omega^2} & \omega \text{ fixed} \\ \frac{mk_F}{\pi^2}\left(-1+\frac{s}{2}\ln\left|\frac{1+s}{1-s}\right|\right) & s=\frac{m\omega}{k_F q} \text{ fixed} \end{cases} \tag{5.116a}$$

$$\mathrm{Im}\, D_0(q,\omega) \underset{q\to 0}{\longrightarrow} \begin{cases} 0 & \omega \text{ fixed} \\ 0 & s \text{ fixed} > 1 \\ -\frac{mk_F s}{2\pi} & s \text{ fixed} < 1 \end{cases} \quad . \tag{5.116b}$$

As the first example, consider the electron gas. Because of the $\frac{1}{q^2}$ behavior of the

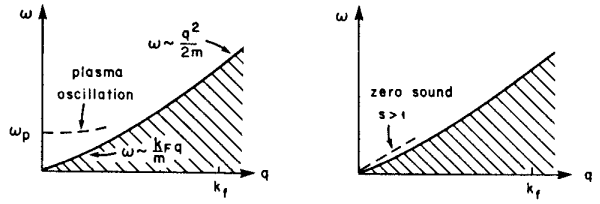

Fig. 5.14 Comparison of plasma oscillation and zero sound mode with the particle-hole continuum.

Coulomb force, we must take the limit in Eq. (5.116a) with finite ω, so that

$$\frac{4\pi e^2}{q^2}\,\frac{k_F^3}{3\pi^2 m}\,\frac{q^2}{\omega^2} = 1 \tag{5.117a}$$

yielding the familiar plasma frequency (see Problem 5.9)

$$\omega_p^2 = \frac{4\pi e^2}{m}\rho \ . \tag{5.117b}$$

The collective RPA mode, or plasmon, is a fundamental excitation of the electron gas which is readily observable experimentally. For example, if one measures the energy loss of electrons in solids, peaks are observed at multiples of ω_p. Since typical Fermi energies in metals are of the order $\epsilon_F \sim 5 - 20\,\text{eV}$, the plasma frequency is in the range $\omega_p \sim 7 - 27\,\text{eV}$. The spectrum of particle-hole excitations within the extremal values $\omega = \frac{q^2}{2m} \pm \frac{qk_F}{m}$ is compared with the plasma frequency in Fig. 5.14. Note that since ω_p is comparable to ϵ_F, the plasma mode is well-isolated from the particle-hole continuum and thus doesn't decay directly through one-particle one-hole states. The leading correction to ω_p, which we have not calculated here, is proportional to q^2

In contrast to the case of the repulsive Coulomb potential, many physical systems have scattering channels in which the interaction is attractive at the Fermi surface, in which case the collective mode is lowered in energy. Consider, for example the case of liquid ^{3}He. On the average, the interaction is repulsive at the Fermi surface since it is the short-range repulsive core of the two-body potential which keeps the liquid from collapsing to higher density. However, although there is negligible explicit spin dependence in the underlying potential, because two ^{3}He atoms in a spin triplet state must be spatially antisymmetric, they feel the hard core much less strongly than two atoms in a singlet state, and the interaction in the triplet channel is overall attractive. Thus, the spin-dependence tends to drive the system toward a ferromagnetic state and manifests itself in a low-energy collective RPA mode known as a paramagnon. In the limit in which the attraction between like spins were strong enough to drive the system ferromagnetic, this mode would occur at zero energy. Although it is not pushed down that far, it makes a significant contribution to the self-energy. In addition to the

Hartree-Fock and second order diagrams discussed in Section 5.3, RPA graphs such as

$\Sigma_{\text{RPA}} =$ 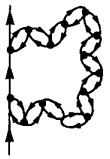 (5.118)

make a dramatic contribution to the effective mass. In the pressure range of 0.3 to 27 atm., $\frac{m^*}{m}$ ranges from 3.1 to 5.8, corresponding to the fact that in order to move a single ^{3}He atom through the medium, one must also drag along a large cluster of atoms with the same spin.

A second example is the case of pion condensation in neutron or nuclear matter at high density (occurring for example in neutron stars). Whereas the ^{3}He–^{3}He interaction is attractive in the $\sigma \cdot \sigma$ channel, by virtue of the spin-isospin coupling of pions to nucleons and the resulting strong tensor forces, the nucleon-nucleon interaction at the Fermi surface is strongly attractive in the $\sigma \cdot \sigma\ \tau \cdot \tau$ channel, giving rise to low energy collective excitations with the quantum numbers of the pion. Although uncertainties in the behavior of strong interactions at high density makes quantitative predictions uncertain, this mode is predicted to have zero energy and thus to lead to pion condensation at a density several times the density of nuclear matter.

ZERO SOUND

We now consider finite-range repulsive potentials, for which the low-q behavior of the collective mode is completely different than for the Coulomb potential. Since non-Coulombic potentials are less singular than $\frac{1}{q^2}$ at low q, the dispersion relation $\tilde{v}D = 1$ cannot be satisfied for a finite ω, so $\omega \to 0$ as $q \to 0$. Thus, modes which go to zero at large wavelength are the general rule, and the finite energy modes such as the plasmon are exceptional cases associated with the infinite range of the force. Note that we have already seen an example of the role of the force range in considering spin waves. Since orienting different spin domains in different directions costs no energy except at the domain boundaries, if the force range is finite, the effect of the boundaries becomes negligible in the long wavelength limit and the energy of such a Goldstone mode must go to zero. Only if the force range is infinite do the boundary contributions remain finite, yielding a finite excitation energy.

To simplify the discussion of the collective mode, which is called zero sound, let us consider the case in which $\tilde{v}(q)$ is independent of q at small q and define

$$f \equiv \tilde{v}(0) = \int d^3r\, v(r) \ . \tag{5.119}$$

We now take the small q limit of the dispersion relation holding s fixed and greater than 1 to obtain real (undamped) solutions

$$\begin{aligned}\frac{1}{f} &= D_0(q,\omega) \\ &\xrightarrow[q\to 0]{} \frac{mk_F}{\pi^2}\left(-1 + \frac{s}{2}\ln\left|\frac{1+s}{1-s}\right|\right)\end{aligned} \tag{5.120}$$

where s defined in Eq. (5.116) is the ratio of the speed of the zero sound mode, $c_0 = \frac{\omega}{q}$, to the Fermi velocity, v_f,

$$s = \frac{\frac{\omega}{q}}{\frac{k_f}{m}} = \frac{c_0}{v_F} \quad . \tag{5.121}$$

Note that solutions with $s > 1$ exist for all positive f, that is, for all repulsive interactions. For large f, (where the simple RPA presented here is an inadequate approximation) we may expand $\ln\left|\frac{1+s}{1-s}\right|$ to obtain

$$\frac{1}{f} \approx \frac{mk_F}{\pi^2}\left[\frac{1}{3s^2} + \frac{1}{5s^4} + \cdots\right] \tag{5.122a}$$

so that

$$s \underset{f\to\infty}{\longrightarrow} \left[\frac{mk_F}{3\pi^2} f\right]^{1/2} \quad . \tag{5.122b}$$

In the limit of small f, s approaches 1 exponentially

$$s \underset{f\to 0}{\longrightarrow} 1 + 2e^{-\frac{2\pi^2}{mk_F f}} \tag{5.122c}$$

and the velocity of zero sound is therefore close to, but slightly above, the Fermi velocity

$$c_0 \approx \frac{k_F}{m} \quad . \tag{5.123}$$

The zero sound mode is sketched in part (b) of Fig. 5.14. Note that the fact $s > 1$ places the mode above the particle-hole continuum and prevents its direct decay through coupling to one-particle, one-hole states.

For comparison, compare this velocity with ordinary thermodynamic sound in a nearly non-interacting Fermi gas in d dimensions in which there are sufficient interactions to produce thermodynamic equilibrium, but these interactions contribute negligibly to the energy per particle. Noting that the Fermi gas energy per particle in d dimensions is $\frac{d}{d+2}\frac{k_F^2}{2m}$ and $\rho \propto k_F^d$, the usual thermodynamic arguments yield the velocity of thermodynamic, or first sound*

$$c_1 = \left[\frac{1}{m}\frac{dP}{d\rho}\right]^{1/2} = \frac{1}{\sqrt{d}}\frac{k_F}{m} \quad . \tag{5.124}$$

Thus, in a weakly interacting system in three dimensions, c_1 is approximately $\frac{1}{\sqrt{3}}c_o$. Furthermore, at least the velocity suggests that the geometry of zero sound may be more one-dimensional than three dimensional, and we will now develop an appropriate language to examine the geometry of zero sound.

* For an infinitesimal change in density, the continuity equation requires $\frac{\partial}{\partial t}\delta\rho + \rho_0\nabla\cdot v = 0$ and Newton's equation of motion requires $m\rho_0\frac{\partial v}{\partial t} = -\nabla P$. Hence, the wave equation is $\frac{\partial^2}{\partial t^2}\delta\rho = \frac{1}{m}\nabla^2 P(\rho_0+\delta\rho) = \frac{1}{m}\frac{\partial P}{\partial\rho}\nabla^2\delta\rho$ and $c^2 = \frac{1}{m}\frac{dP}{\delta\rho}$.

Since zero sound is a coherent superposition of particle-hole excitations near the Fermi surface, we would like to simultaneously examine the behavior in momentum space and coordinate space. If we were dealing with a classical system, it would be natural to study its classical distribution function as a function of coordinates and momenta. For a quantal system, the best analog of the classical distribution function is the Wigner function and for our present purposes it is most useful to study the Wigner transform of the one-body density matrix:

$$f(\vec{p},\vec{R}) = \int d^3r\, e^{-i\vec{p}\cdot\vec{r}}\left\langle\psi^\dagger\left(\vec{R}-\tfrac{\vec{r}}{2}\right)\psi\left(\vec{R}-\tfrac{\vec{r}}{2}\right)\right\rangle \quad . \tag{5.125}$$

In addition to yielding the familiar distribution function in the classical limit, its moments have the following properties associated with the classical distribution function:

$$\begin{aligned}
\int\frac{d^3p}{(2\pi)^3}f(\vec{p},\vec{R}) &= \langle\psi^\dagger(\vec{R})\psi(\vec{R})\rangle = \langle\hat{\rho}(\vec{R})\rangle \\
\int d^3R\, f(\vec{p},\vec{R}) &= \int d^3r\, d^3R\, e^{-i\vec{p}\left(\vec{R}+\frac{\vec{r}}{2}\right)}\, e^{i\vec{p}\cdot\left(\vec{R}-\frac{\vec{r}}{2}\right)}\left\langle\psi^\dagger\left(\vec{R}-\tfrac{\vec{r}}{2}\right)\rho\left(\vec{R}+\tfrac{\vec{r}}{2}\right)\right\rangle \\
&= \langle a_p^\dagger a_p\rangle = \langle\hat{\rho}_p\rangle \\
\int\frac{d^3p}{(2\pi)^3}\frac{\vec{p}}{m}f(\vec{p},\vec{R}) &= \int\frac{d^3p}{(2\pi)^3}d^3r\, e^{-i\vec{p}\cdot\vec{r}}\left\langle\frac{1}{im}\vec{\nabla}_R\left\{\psi^\dagger\left(\vec{R}-\tfrac{\vec{r}}{2}\right)\psi\left(\vec{R}+\tfrac{\vec{r}}{2}\right)\right\}\right\rangle \\
&= \frac{1}{2mi}\left\langle\psi^\dagger(\vec{R})\vec{\nabla}_R\psi(R) - \left(\nabla_R\psi^\dagger(\vec{R})\right)\psi(\vec{R})\right\rangle \\
&= \langle\hat{j}(R)\rangle
\end{aligned} \tag{5.126}$$

and similarly for higher moments. Essentially the only property $f(\vec{r},\vec{R})$ does not share with the classical distribution function is positivity, and this deficiency will not affect the present argument.

Now, let us use the RPA response function to look at the response of the Wigner transform of the one-body density operator to a weak perturbation $\delta U(t_2)\rho_q(t_2)$ which couples to the zero sound mode. Using Eq. (2.15) and omitting the standard details in going from the retarded to time-ordered response function, which are irrelevant to the present point,

$$\begin{aligned}
\delta f(\vec{p},\vec{R};t) &= -i\int dt_2\delta U(t_2)\int dr\, e^{-i\vec{p}\cdot\vec{r}}\langle T\psi^\dagger\left(\vec{R}-\frac{\vec{r}}{2},t_1\right)\psi\left(\vec{R}+\frac{\vec{r}}{2},t_1\right)\times \\
&\quad\times a^\dagger_{\vec{k}_2+\vec{q}}(t_2)a_{\vec{k}_2}(t_2)\rangle \\
&= -i\int dt_2\delta U(t_2)\int dr\, e^{-i\vec{p}\cdot\vec{r}}\sum_{k_1k'}e^{-i\vec{k}_1\cdot\left(\vec{R}-\frac{\vec{r}}{2}\right)}\, e^{i\vec{k}'\left(\vec{R}+\frac{\vec{r}}{2}\right)} \\
&\quad\times\delta(\vec{k}_1+\vec{q}-\vec{k}')\left\langle Ta^\dagger_{\vec{k}_1}(t_1)a_{\vec{k}_1+\vec{q}}(t_1)a^\dagger_{\vec{k}_2+\vec{q}}(t_2)a_{\vec{k}_2}(t_2)\right\rangle \quad .
\end{aligned} \tag{5.127}$$

Noting that the zero sound pole arises from the second term in Eq. (5.113) and that the only dependence on k_1 enters through $G_0^{\rm ph}(k_1,q,\omega)$, substitution of the RPA response

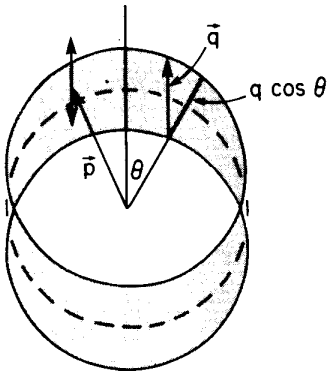

Fig. 5.15 Phase space contributing to $G_0^{\rm ph}\left(\vec{p}-\frac{\vec{q}}{2}\right)$. The centers of the two solid spheres are displayed $\pm\frac{\vec{q}}{2}$ relative to the dashed Fermi sphere. Every vector $\vec{p}$ in the upper shaded region yields $\vec{p}+\frac{\vec{q}}{2}$ outside the dashed sphere and $\vec{p}-\frac{\vec{q}}{2}$ inside.

function in Eq. (5.127) yields

$$\begin{aligned}\delta f(\vec{p},\vec{R};\omega) &\propto \int dr\; e^{-i\vec{p}\cdot\vec{r}}\sum_{k_1} e^{-i\vec{k}_1\cdot\left(\vec{R}-\frac{\vec{r}}{2}\right)}\; e^{i(\vec{k}_1+\vec{q})\cdot\left(\vec{R}+\frac{\vec{r}}{2}\right)}G_0^{\rm ph}(\vec{k}_1)\\ &= e^{i\vec{q}\cdot\vec{R}}G_0^{\rm ph}\left(\vec{p}-\frac{\vec{q}}{2}\right) \qquad (5.128)\\ &= e^{i\vec{q}\cdot\vec{R}}\,\frac{(1-n_{\vec{p}+\frac{\vec{q}}{2}})n_{\vec{p}-\frac{\vec{q}}{2}}-(1-n_{\vec{p}-\frac{\vec{q}}{2}})n_{\vec{p}+\frac{\vec{q}}{2}}}{\omega+\epsilon_{\vec{p}-\frac{\vec{q}}{2}}-\epsilon_{\vec{p}+\frac{\vec{q}}{2}}}\ .\end{aligned}$$

For small $\vec{q}$, the range of $\vec{p}$ which satisfy the conditions that $\vec{p}\pm\frac{\vec{q}}{2}$ be outside the Fermi sphere while $p\mp\frac{q}{2}$ be inside can be calculated easily from the geometrical construction shown in Fig. 5.15. The shaded region defining the vectors $\vec{p}$ such that $\vec{p}\pm\frac{\vec{q}}{2}$ lies outside the dashed Fermi sphere while $\vec{p}\mp\frac{\vec{q}}{2}$ lies inside have radial thickness $q\cos\theta$ where θ is the angle between $\vec{p}$ and $\vec{q}$. Since the p's are all confined to be close to the Fermi surface, we may write the phase space factor as $\delta(k_F-|\vec{p}|)q\cos\theta$. Finally, writing the denominator as $\omega+\epsilon_{p-\frac{q}{2}}-\epsilon_{p+\frac{q}{2}}=\frac{sqk_F}{m}-\frac{qk_F\cos\theta}{m}$ and writing the explicit time-dependence, we obtain the desired result.

$$\delta f(\vec{p},\vec{R},t)\propto e^{i(\vec{q}\cdot\vec{R}-\omega t)}\,\frac{\delta(k_F-|\vec{p}|)\cos\theta}{s-\cos\theta}\ . \qquad (5.129)$$

This result is also obtained using Landau Fermi Liquid Theory in Chapter 6. The factor $\frac{\cos\theta}{s-\cos\theta}$ specifies the change in the distribution function as a function of the angle between $\vec{p}$ and $\vec{q}$. Since s is close to 1, the magnitude of the peak at $\theta=0$ is much larger than at $\theta=\pi$, so the volume of the Fermi sphere and thus the local density changes.

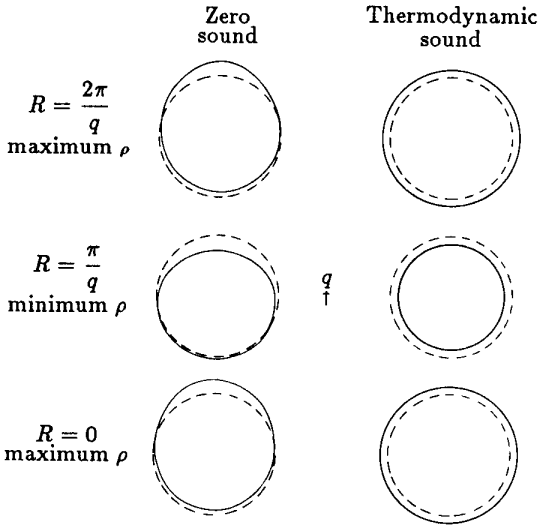

Fig. 5.16 The distribution function $f(p,R)$ for zero sound and thermodynamic sound. The equilibrium Fermi sphere is shown at each spatial position by the dashed line and the solid line denotes the momentum distribution of the propagating mode.

Figure 5.16 compares the evolution of the distribution function for zero sound with that of thermodynamic sound. The factor $e^{i(\vec{q}\cdot\vec{R}-\omega t)}$ propagates the fluctuation of the zero sound distribution function in the $\vec{q}$ direction at speed $v_0=s\frac{k_F}{m}$. Snapshots are shown of the momentum distribution at spatial points R separated by a half wavelength. The origin is selected such that the density is a maximum at $R=0$, so the Fermi sphere distorts at successive displacements of $\frac{\pi}{q}$ by adding or subtracting $\frac{\cos\theta}{s-\cos\theta}$. The distribution is thus highly anisotropic and is concentrated in the forward $\vec{q}$ direction. In contrast, the Fermi sphere for thermodynamic sound just dilates and contracts spherically symmetrically. To the extend to which the zero sound distortion is concentrated in the longitudinal direction and the transverse radius of the Fermi surface is unaffected, the mode is more like one-dimensional thermodynamic sound than three-dimensional thermodynamic sound, consistent with Eq. (5.124).

Zero sound and thermodynamic sound thus represent two opposite extremes. Zero sound is built out of quasiparticles, so at finite temperatures the frequency must be high enough that the quasiparticles do not decay, that is, that collisions do not dominate. Quasiparticles travelling in the $\vec{q}$ direction are thus not scattered in the transverse directions and the mode can remain essentially one-dimensional. At zero temperature, for which we have performed our calculation, the lifetime becomes infinite as quasiparticles approach the Fermi surface, so zero sound propagates at all frequencies. In contrast, thermodynamic sound requires local equilibrium. Hence, the frequency must

be low enough that collisions dominate and quasiparticles and collective modes decay. Longitudinal momentum is equilibrated with transverse momentum, so that the Fermi surface is necessarily isotropic and the mode is fully three-dimensional. In liquid ^{3}He, one may experimentally observe the transition from zero sound to thermodynamic sound by varying the frequency and the temperature between collision-free and collision-dominated regimes.

MATRIX FORM OF RPA

Additional physical insight into the RPA may be obtained by deriving it from the time-dependent Hartree-Fock approximation, discussed in Problem (5.10). To make contact with this and other approaches, it is useful to write the RPA equations in their conventional matrix form. To display their full generality, instead of working in momentum space, we will work in a general basis with our usual convention of unoccupied states $\{a, b \cdots\}$, occupied states $\{A, B \cdots\}$, and arbitrary states $\{\alpha, \beta \cdots\}$. Rewriting Eq. (5.112) so as to distinguish the two possible cases $G^{\rm RPA}(aA|\alpha\beta)$ and $G^{\rm RPA}(Aa|\alpha\beta)$ we obtain the two equations

$$G^{\rm RPA}(aA|\alpha\beta;\omega) = \frac{1}{\omega+\epsilon_A-\epsilon_a+i\eta}\Big[\delta_{a\alpha}\delta_{A\beta} + \sum_{bB}\{aB|v|Ab\}\,G^{\rm RPA}(bB|\alpha\beta;\omega) + \sum_{bB}\{ab|v|AB\}\,G^{\rm RPA}(Bb|\alpha\beta;\omega)\Big] \tag{5.130}$$

$$G^{\rm RPA}(Aa|\alpha\beta;\omega) = \frac{-1}{\omega+\epsilon_a-\epsilon_A-i\eta}\Big[\delta_{A\alpha}\delta_{a\beta} + \sum_{bB}\{AB|v|ab\}\,G^{\rm RPA}(bB|\alpha\beta;\omega) + \sum\{Ab|v|aB\}\,G^{\rm RPA}(Bb|\alpha\beta;\omega)\Big] \ .$$

With the definitions

$$\begin{aligned} A_{AaBb} &= (\epsilon_a-\epsilon_A)\delta_{AB}\delta_{ab} + \{aB|v|Ab\} \\ B_{AaBb} &\equiv \{ab|v|AB\} \end{aligned} \tag{5.131}$$

these equations may be written in the matrix form

$$\begin{pmatrix} -\omega+A & B \\ B^* & \omega+A^* \end{pmatrix}\begin{pmatrix} G(bB|\alpha\beta;\omega) \\ G(Bb|\alpha\beta;\omega)\end{pmatrix} = \begin{pmatrix} -\delta_{a\alpha}\delta_{A\beta} \\ -\delta_{A\alpha}\delta_{a\beta}\end{pmatrix} \ . \tag{5.132}$$

The poles of G are given by the eigenvalues of the generalized eigenvalue problem (note the minus sign on the right-hand side):

$$\begin{pmatrix} A & B \\ B^* & A^*\end{pmatrix}\begin{pmatrix} X^{(\nu)} \\ Y^{(\nu)}\end{pmatrix} = E^{(\nu)}\begin{pmatrix} X^{(\nu)} \\ -Y^{(\nu)}\end{pmatrix} \tag{5.133}$$

where $X^{(\nu)}$ is a column of elements $X^{(\nu)}_{bB}$ labeled by particle-hole labels $\{b, B\}$. Using the properties established in Problem (5.11), the particle-hole Green's function may be

written as a sum over all positive energy modes

$$G^{\rm RPA} = \sum_\nu \frac{\begin{pmatrix} X^{(\nu)} \\ Y^{(\nu)}\end{pmatrix}(X^{(\nu)\dagger}Y^{(\nu)\dagger})}{\omega-E^{(\nu)}+i\delta} - \frac{\left[\begin{pmatrix} Y^{(\nu)} \\ X^{(\nu)}\end{pmatrix}(Y^{(\nu)\dagger}X^{(\nu)\dagger})\right]^*}{\omega+E^{(\nu)}-i\delta} \ . \tag{5.134}$$

Since this is a spectral representation for the RPA response function of the same form as Eq. (5.100) for the exact response function, the $X^{(\nu)}$ and $Y^{(\nu)}$ should correspond to matrix elements of $a^\dagger_\alpha a_\beta$ between RPA approximates to the excited states, denoted $|\psi^{\rm RPA}_\nu\rangle$, and the RPA ground state, denoted $|\psi^{\rm RPA}_0\rangle$. Noting that the upper component $G^{\rm RPA}(bB|\alpha\beta)$ involves the matrix element $\langle a^\dagger_B a_b a^\dagger_\alpha a_\beta\rangle$ and $G^{\rm RPA}(Bb|\alpha\beta)$ corresponds to $\langle a^\dagger_b a_B a^\dagger_\alpha a_\beta\rangle$, it follows that

$$\begin{aligned} \left(X^{(\nu)}_{bB}\right)^* &= \langle\psi^{\rm RPA}_\nu|a^\dagger_b a_B|\psi^{\rm RPA}_0\rangle \\ Y^{(\nu)}_{bB} &= \langle\psi^{\rm RPA}_\nu|a^\dagger_B a_b|\psi^{\rm RPA}_0\rangle \ . \end{aligned} \tag{5.135}$$

If $|\psi^{\rm RPA}_0\rangle$ were just the non-interacting ground state, $a^\dagger_B a_b$ would annihilate it yielding $Y^{(\nu)} = 0$. However, from Problems (5.5) and (5.10) it is clear that the RPA ground state contains multi particle-hole admixtures which produce a non-vanishing $Y^{(\nu)}$ amplitude. Equations (5.134– 5.135) thus relate the two distinct random phase approximations alluded to earlier for the response function and for individual eigenstates.

SUM RULES AND EXAMPLES

We conclude this section by stating several sum rules satisfied by the response function and presenting illustrative physical examples.

In addition to dispersion relations of the form of (5.35) which follow directly from the spectral representation of D, the imaginary part of the response function satisfies two important sum rules. The first follows from integrating out the energy conserving δ-function and using completeness and the field operator commutation relation

$$\begin{aligned} \int d\omega \,\mathrm{Im}\, D(x_1,x_2;\omega) &= -\pi\sum_n \int d\omega\,\delta(\omega-E^N_n+E_0) \\ &\quad\times\langle\psi_0|(\hat\rho(x_1)-\langle\hat\rho(x_1)\rangle)|\psi_n\rangle\langle\psi_n|(\hat\rho(x_2)-\langle\hat\rho(x_2)\rangle|\psi_0\rangle \\ &= -\pi\big[\langle\rho(x_1)\rho(x_2)\rangle - \langle\rho(x_1)\rangle\langle\rho(x_2)\rangle\big] \\ &= -\pi[g(x_1,x_2)+\delta(x_1-x_2)\rho(x_1)] \end{aligned} \tag{5.136}$$

where $g(x_1,x_2)$ is the two-body correlation function

$$g(x_1,x_2) \equiv \langle\psi_0\,|\psi^\dagger(x_1)\psi^\dagger(x_2)\psi(x_2)\psi(x_1)|\,\psi_0\rangle - \langle\psi_0\,|\hat\rho(x_1)|\,\psi_0\rangle\,\langle\psi_0\,|\hat\rho(x_2)|\,\psi_0\rangle \ . \tag{5.137}$$

In momentum space, where $g(x_1,x_2) = g(x_1-x_2)$

$$\begin{aligned} -\frac{1}{\pi N}\int d\omega\,\mathrm{Im}\,D(q,\omega) &\equiv S(q) \\ &= \rho\int dx\, e^{-iq\cdot x}g(x) + 1 \ . \end{aligned} \tag{5.138}$$

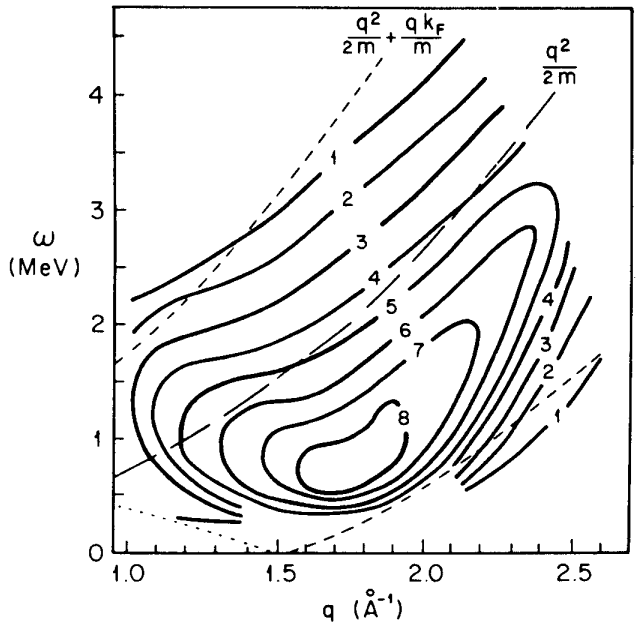

Fig. 5.17 Sketch of cross section for inelastic neutron scattering from liquid ^{3}He based on the data of Stirling *et al* (1976). Solid contours denote the experimental cross sections, the long dashed curve indicates the Fermi gas maximum, $\frac{q^2}{2m}$, the short dashed curves show where the Fermi gas response goes to zero, $\frac{q^2}{2m} \pm \frac{qk_F}{m}$, and the dotted line denotes the point at which Pauli blocking begins.

Since $\mathrm{Im}\, D(q,\omega)$ is directly measurable in inclusive scattering, Eq.. (5.138) shows that one may measure the Fourier transform of the two-body correlation function by simply integrating over ω.

An energy weighted sum rule is derived in Problem 5.13 by evaluating the expectation value of the double commutator $\langle[[H,\hat{\rho}_q],\rho_{-q}]\rangle$ with the result

$$-\frac{1}{\pi N}\int d\omega\,\omega\,\mathrm{Im}\,D(q,\omega) = \frac{q^2}{2m} \quad . \tag{5.139}$$

A variety of useful related sum rules may be obtained by choosing other operators in the double commutator instead of $\hat{\rho}_q$. For example, one may take the electric dipole transition operator and relate the integral of the dipole transition strength for a finite nucleus to the charge radius (plus corrections for velocity dependent and isospin dependent terms). This gives a total sum with which to compare the strength of an individual transition. The giant dipole resonance is "giant" because its strength exhausts most of the sum rule.

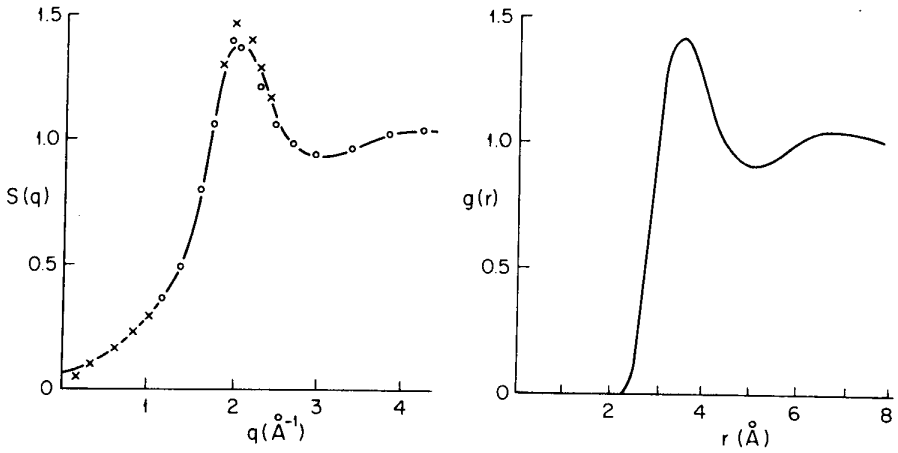

Fig. 5.18 Liquid structure function $S(q)$ and two-body correlation function $g(r)$ for liquid ^{4}He. The left-hand graph compares X-ray scattering data of Hallock (1972) and Rubkoff *et al.* (1979) (crosses) and neutron scattering data of Svensson *et al.* (1980) (circles) with the structure function obtained from Monte Carlo calculations (solid curves) of Kalos *et al.* (1981). The right-hand graph shows the two-body correlation function corresponding to this $S(q)$.

Experimental measurements of response functions for several physical systems are presented in Figs. 5.17 – 5.19. Fig. 5.17 shows a contour plot in the (q,ω) plane of the cross section for inelastic scattering of neutrons from liquid ^{3}He at 0.63° K (Stirling *et al.*, 1976). Since the neutron-^{3}He potential is effectively a δ-function on the scale of Angstroms relevant to the experiment, the cross section is directly proportional to $\mathrm{Im}\, D(q,\omega)$. Using the value of $k_F = 0.786$ Å^{-1} specified by the ground state density, the maximum $\frac{q^2}{2m}$ and zeros $\frac{q^2}{2m} \pm \frac{qk_F}{m}$ expected from $D_0(q,\omega)$ are indicated by dashed lines. Although the data has the qualitative structure of D_0, it differs quantitatively in detail. In particular, one sees clear evidence of a large enhancement in the effective mass. The experimental peak in the region of $q \sim 2k_F$ occurs at $\sim \frac{1}{3} \times \frac{q^2}{2m}$ so that $m^* \sim 3m$.

The structure factor for liquid ^{4}He, $S(q)$ defined in Eq. (5.138), has been measured both by X-ray scattering (Hallock, 1972; Robkoff *et al.* 1979) and neutron scattering (Svensson *et al.* 1980) Typical data are shown in Fig. 5.18, and are observed to agree quite well with each other and with the results obtained from Monte Carlo solution of the zero-temperature ground state of ^{4}He (Kalos *et al.* 1981) using the Aziz (1979) potential. As discussed in Chapter 8, the Monte Carlo solution provides an essentially exact solution for the ground state of N particles in a box with periodic boundary conditions, so the only error in the structure function is the departure from linearity at very low q associated with the finite box size. One thereby has an exceedingly pre-

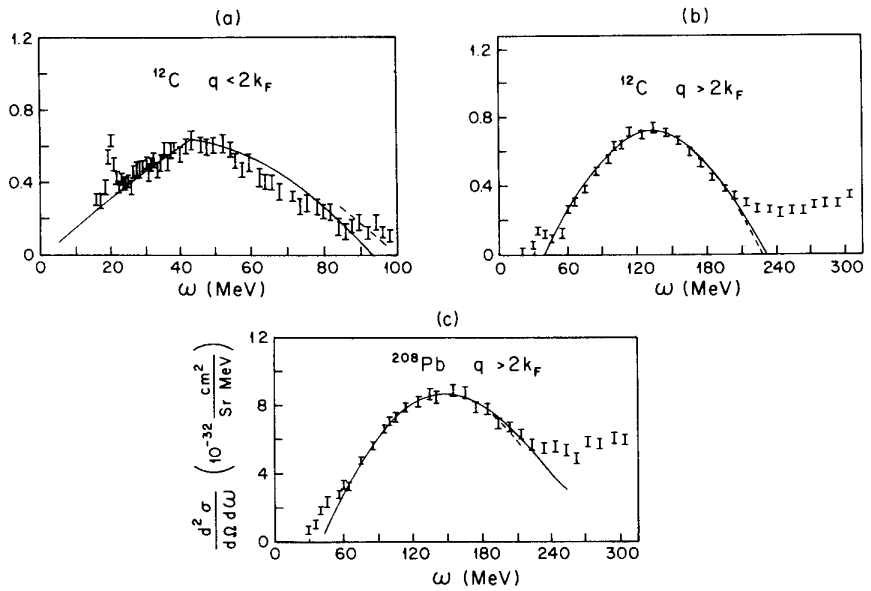

Fig. 5.19 Inclusive electron scattering from atomic nuclei. The inclusive cross sections as a function of energy loss ω for ^{12}C at incident energy $E = 198.5\,\text{MeV}$ and scattering angle $\theta = 135°$ in (a) correspond to momentum transfer q less than $2k_F$ whereas the $E = 500\,\text{MeV}$ data at $\theta = 60°$ shown for ^{12}C in (b) and ^{208}Pb in (c) correspond to momentum transfer greater than $2k_F$. The solid curves correspond to the Fermi gas response functions described in the text. The low energy data is from Leiss and Taylor (1963) and the high energy data from Moniz *et al.* (1971).

cise measurement of the two-body correlation function of a dense, strongly interacting quantum liquid, also shown in Fig. 5.18. One observes in particular the strong suppression of the wave function at short distance due to the strongly repulsive core of the He–He potential. Note that the strength of the interaction between the constituents in no way affects the applicability of the linear response analysis: all that matters is that the coupling of the external probe, in this case the X-ray or neutrons, is weak.

A final example is inelastic electron scattering from atomic nuclei, shown in Fig. 5.19. A good approximation to the response may be obtained using the response function for a non-interacting Fermi gas corrected for the medium dependence of the nucleon self-energy. Recall from Fig. 5.12 that when the momentum transfer $q > 2k_F$, there is no Pauli blocking and $\text{Im}\, D_0(q,\omega)$ is an inverted parabola with center at $\omega = \frac{q^2}{2m}$ and width $\frac{2qk_F}{m}$. In contrast, when $q < 2k_F$, Pauli blocking yields linear dependence below $\omega = \frac{qk_F}{m} - \frac{q^2}{2m}$. This qualitative difference is observed in the low and high momentum transfer data for ^{13}C in (a) and (b) and the high momentum transfer data for ^{208}Pb in (c). Note that the excess cross section at high ω corresponds to the inelastic processes in which pions or Δ resonances are produced. In Section 5.3, we saw that the nuclear self-energy was strongly momentum dependent, with a nucleon within the Fermi sea having a strong attraction and nucleons well above the Fermi sea having much weaker attraction. This effect may be included approximately in the response function either by introducing an effective mass m^* or a binding correction $\bar{\epsilon}$ representing the average difference between the self-energy of a nucleon in and outside the Fermi sea. In either case, the data specify two parameters, k_F and either m^* or $\bar{\epsilon}$. The ^{12}C data of Leiss and Taylor (1960) in (a) are fit with $k_F = 1.19\,\text{fm}^{-1}$ and $m^*/m = 0.7$ (Moniz 1969), consistent with the value m^*/m discussed in Section 5.3 and the fact that the average Fermi momentum in a small, surface dominated nucleus like ^{12}C is somewhat lower than the value $k_F = 1.31$ in fm^{-1} in bulk nuclear matter. The high momentum transfer data for ^{12}C in (b) is fit with $k_F = 1.14\,\text{fm}^{-1}$ and $\bar{\epsilon} = 25\,\text{MeV}$ (Moniz *et al.*, 1971) consistent with the previous value of k_F and the fact that the average of the observed single particle energies is of the order of 25 MeV. Finally, the same analysis of the ^{208}Pb data yields $k_F = 1.36\,\text{fm}^{-1}$, in satisfactory agreement with bulk matter, and $\bar{\epsilon} = 44\,\text{MeV}$ consistent with the average single-particle energy in ^{208}Pb. Thus, the Fermi gas response corrected for the known behavior of the self-energy gives a simple semi-quantitative physical description of the nuclear response function.

5.5 MAGNETIC SUSCEPTIBILITY OF A FERMI GAS

The magnetic susceptibility of a non-interacting Fermi gas is an instructive, illustrative application of many of the ideas presented in this chapter. Although the problem is in some aspects trivial, because it is an exactly solvable problem with one-body interactions, it clearly demonstrates the similarities and differences between zero and finite temperatures and between static and dynamic response. In addition, it will demonstrate some of the techniques involved in practical calculations.

The specific model to be solved is a system of non-interacting spin-1/2 Fermions coupled to a constant external magnetic field in the $\hat{z}$ direction

$$\begin{aligned} V_{\alpha\beta} &= -\mu_0 H \sigma^{(z)}_{\alpha\beta} \\ V_{\alpha\beta}(q) &= -\mu_0 \sigma^{(z)}_{\alpha\beta} (2\pi)^3 \delta^3(q) \end{aligned} \tag{5.140}$$

where α, β denote spin indices, μ_0 is the magnetic moment and $\sigma^{(z)}$ is a Pauli spin matrix. We will now calculate the susceptibility four different ways and compare the results.

STATIC SUSCEPTIBILITY AT ZERO TEMPERATURE

The magnetic susceptibility is

$$\chi = \left.\frac{\partial \langle M \rangle}{\partial H}\right|_{H\to 0} \tag{5.141}$$